Article

Structural Evolution and Electronic Properties of Two Sulfur Atom-Doped Boron Clusters

Shi-Xiong Li,* Yue-Ju Yang, and De-Liang Chen

Read Online

ACCESS | Metrics & More | Article Recommendations | SI Supporting Information

ABSTRACT: We present a theoretical study of structural evolution, electronic properties, and photoelectron spectra of two sulfur atom-doped boron clusters $S_2B_n^{0/-}$ ($n = 2-13$), which reveal that the global minima of the $S_2B_n^{0/-}$ ($n = 2-13$) clusters show an evolution from a linear-chain structure to a planar or quasi-planar structure. Some S-doped boron clusters have the skeleton of corresponding pure boron clusters; however, the addition of two sulfur atoms modified and improved some of the pure boron cluster structures. Boron is electron-deficient and boron clusters do not form linear chains. Here, two sulfur atom doping can adjust the pure boron clusters to a linear-chain structure ($S_2B_2^{0/-}$, $S_2B_3^{0/-}$, and $S_2B_4^-$), a quasi-linear-chain structure ($S_2B_6^-$), single- and double-chain structures (S_2B_6 and $S_2B_9^-$), and double-chain structures (S_2B_5, and S_2B_9). In particular, the smallest linear-chain boron clusters $S_2B_2^{0/-}$ are shown with an S atom attached to each end of B_2. The S_2B_2 cluster possesses the largest highest occupied molecular orbital (HOMO)−lowest unoccupied molecular orbital (LUMO) gap of 5.57 eV and the $S_2B_2^-$ cluster possesses the largest average binding energy E_b of 5.63 eV, which shows the superior chemical stability and relative stability, respectively. Interestingly, two S-atom doping can adjust the quasi-planar pure boron clusters (B_7^-, B_{10}^-, and $B_{12}^{0/-}$) to a perfect planar structure. AdNDP bonding analyses reveal that linear S_2B_3 and planar SeB_{11}^- have π aromaticity and σ antiaromaticity; however, S_2B_2, planar S_2B_6, and planar $S_2B_7^-$ clusters have π antiaromaticity and σ aromaticity. Furthermore, AdNDP bonding analyses reveal that planar S_2B_4, S_2B_{10}, and S_2B_{12} clusters are doubly (π and σ) aromatic, whereas $S_2B_5^-$, S_2B_8, $S_2B_9^-$, and $S_2B_{13}^-$ clusters are doubly (π and σ) antiaromatic. The electron localization function (ELF) analysis shows that $S_2B_n^{0/-}$ ($n = 2-13$) clusters have different electron delocalization characteristics, and the spin density analysis shows that the open-shell clusters have different characteristics of electron spin distribution. The calculated photoelectron spectra indicate that $S_2B_n^-$ ($n = 2-13$) have different characteristic peaks that can be compared with future experimental values and provide a theoretical basis for the identification and confirmation of these doped boron clusters. Our work enriches the new database of geometrical structures of doped boron clusters, provides new examples of aromaticity for doped boron clusters, and is promising to offer new ideas for nanomaterials and nanodevices.

Typical regulation of boron clusters by two sulfur atoms.
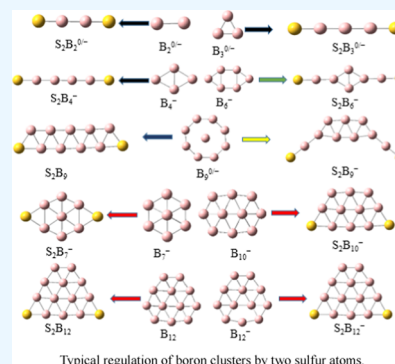
1. INTRODUCTION

Clusters are special aggregates of two or more atoms connected by covalent, metallic, or ionic bonds, and the structures and properties are different from those of bulk materials. The cluster has a series of special properties such as structural specificity, physical and chemical activities, quantum effects, and hydrogen storage performance. In the field of physical chemistry, cluster research has become a hot topic. The pure boron clusters composed of boron atoms with three valence electrons have the characteristic of multicenter bonds and various unique structures and properties.[1−6] Research shows that anionic B_n^- ($n < 38$) presents quasi-planar or planar structures[7,8] and neutral boron clusters present abundant geometric structures.[1,5,9−11] In 2014, the breakthrough discovery of borospherene[12] B_{40}^- has given rise to a lot of research on boron clusters.[13−21] In 2015, two-dimensional borophene was synthesized experimentally,[22] and the basic unit forming borophene happened to be a B_7 cluster. In 2021, a borophene crystal form comparable to graphene was synthesized experimentally;[23] interestingly, the basic structural

unit happened to be a hydrogenated B_7 cluster. The discovery of borospherene and borophene provides important clues for the development of new boron materials.

Doped boron clusters are compounds that embed other atoms into the structure of boron clusters. The addition of these atoms can regulate the structure of boron clusters and then affect the photoelectric properties, magnetic properties, hydrogen storage properties, and other physical and chemical properties of boron clusters. In recent years, researchers have mainly focused on the structure and properties of boron clusters doped with metal atoms.[15,17−19,24−39] For example, single alkali metal atom doping can adjust the quasi-planar

30757

https://doi.org/10.1021/acsomega.3c04967
ACS Omega 2023, 8, 30757−30767
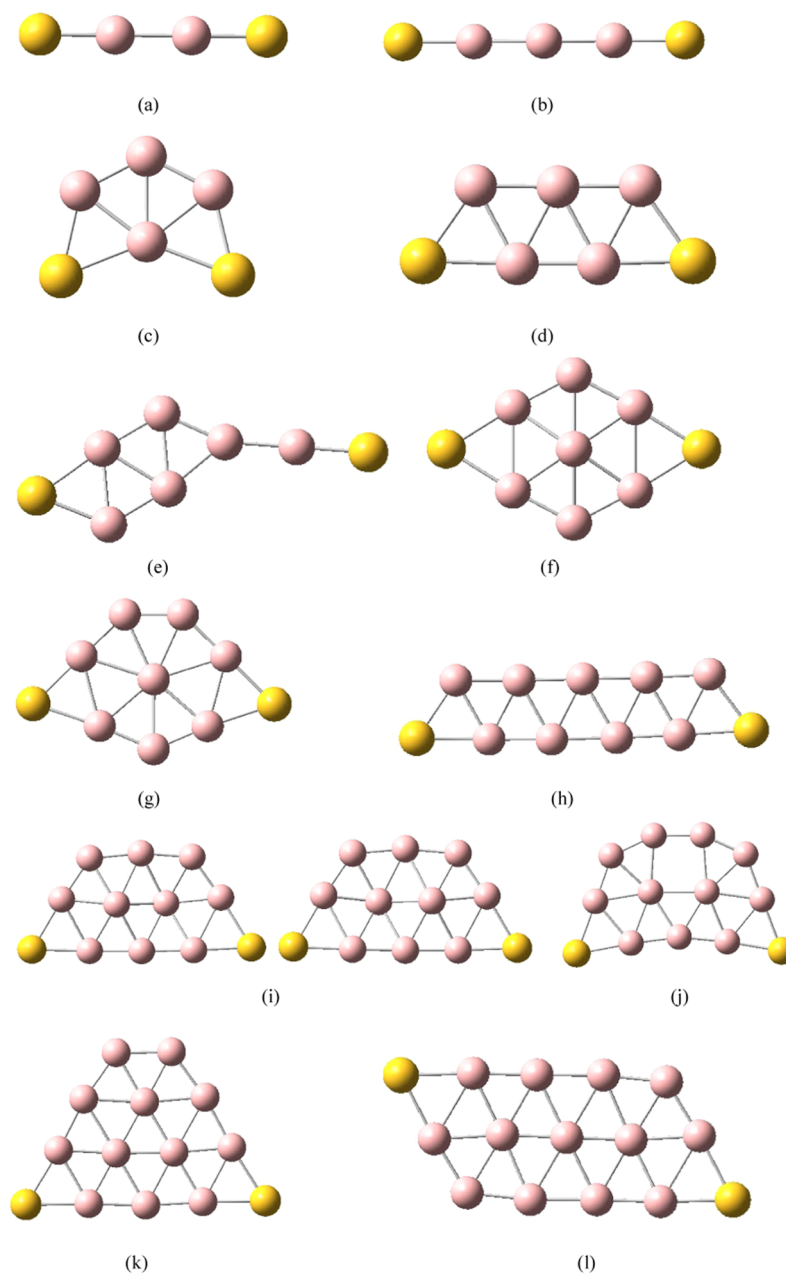
Figure 1. Structures of double S-atom-doped boron clusters S_2B_n ($n = 2-13$). (a) S_2B_2 $D_{\infty h}$; (b) S_2B_3 $D_{\infty h}$; (c) S_2B_4 C_{2v}; (d) S_2B_5 C_{2v}; (e) S_2B_6 C_s; (f) S_2B_7 C_{2v}; (g) S_2B_8 C_{2v}; (h) S_2B_9 C_{2v}; (i) S_2B_{10} C_2; (j) S_2B_{11} C_2; (k) S_2B_{12} C_{2v}; and (l) S_2B_{13} C_2.

pure boron clusters (B_{20}^- and B_{22}^-) to double-ring tubular doped boron clusters (LiB_{20}^-, NaB_{22}^- and KB_{22}^-).[7,25,40,41] Single transition metal atom doping can adjust quasi-planar $B_{12}^{0/-}$ to semisandwich structure CoB_{12}, RhB_{12} and TaB_{12}^-,[3,24,423,24,42] adjust double-ring tubular B_{24} to cage-doped boron clusters (TiB_{24}) and three-ring tubular doped boron clusters (ScB_{24}),[40,43,44] adjust quasi-planar B_{24}^- to cage-doped boron clusters (TiB_{24}^- and VB_{24}^-).[7,45] In addition, doped borospherenes MB_{40} (M = Li, Na, or K) are expected to be applied in nonlinear optical materials,[18] doped borospherenes CoB_{40} and MB_{40} (M = Sc, Ti) are expected to be applied in molecular devices and hydrogen storage materials,[15,17,19,26] and Co- and Rh-doped boron clusters MB_{12} (M = Co, Rh) can improve chemical activity.[27] Single metal atom-doped boron clusters BiB_n^- ($n = 6-8$), MnB_n^- ($n = 6, 16$), and ReB_n^- ($n = 3-4, 6, 8-9$), CoB_{16}^- and two or three metal atom-doped

boron clusters (M_2B_6 (M = Mg, Ca, Sr), $La_2B_{10}^-$, $La_2B_{11}^-$, $La_3B_{18}^-$, and Sc_3B_{20}) have various unique structures.[29-37,46,47] Single Pr atom-doped PrB_4^- can adjust the Pr atom to a very low oxidation state (OS)[48] and single Pr atom-doped PrB_n ($n = 7-16$) have various unique structures;[49] two metal atom-doped boron clusters $Be_2B_{24}^+$ have a four-ring tubular structure.[50] However, nonmetallic atom-doped boron clusters have been less studied,[51-56] such as single O atom doping can adjust the quasi-planar pure boron cluster (B_{12}) to a low-symmetry (C_1) $B_{12}O$ cluster[53] and different numbers of F atom doping can adjust the quasi-planar pure boron cluster (B_{12}) to various unique structures.[51] In addition, there are some related studies on boron oxide clusters and boron sulfide clusters, such as the $B_6(BO)_7^-$ cluster with a face-capping μ^3-BO,[55] planar $B_3S_2H_3$ and $B_3S_2H_3$ clusters with a five-membered B_3S_2 ring,[56] B_6S_6, $B_6S_6^-$, and $B_6S_6^{2-}$ clusters with a planar dicyclic
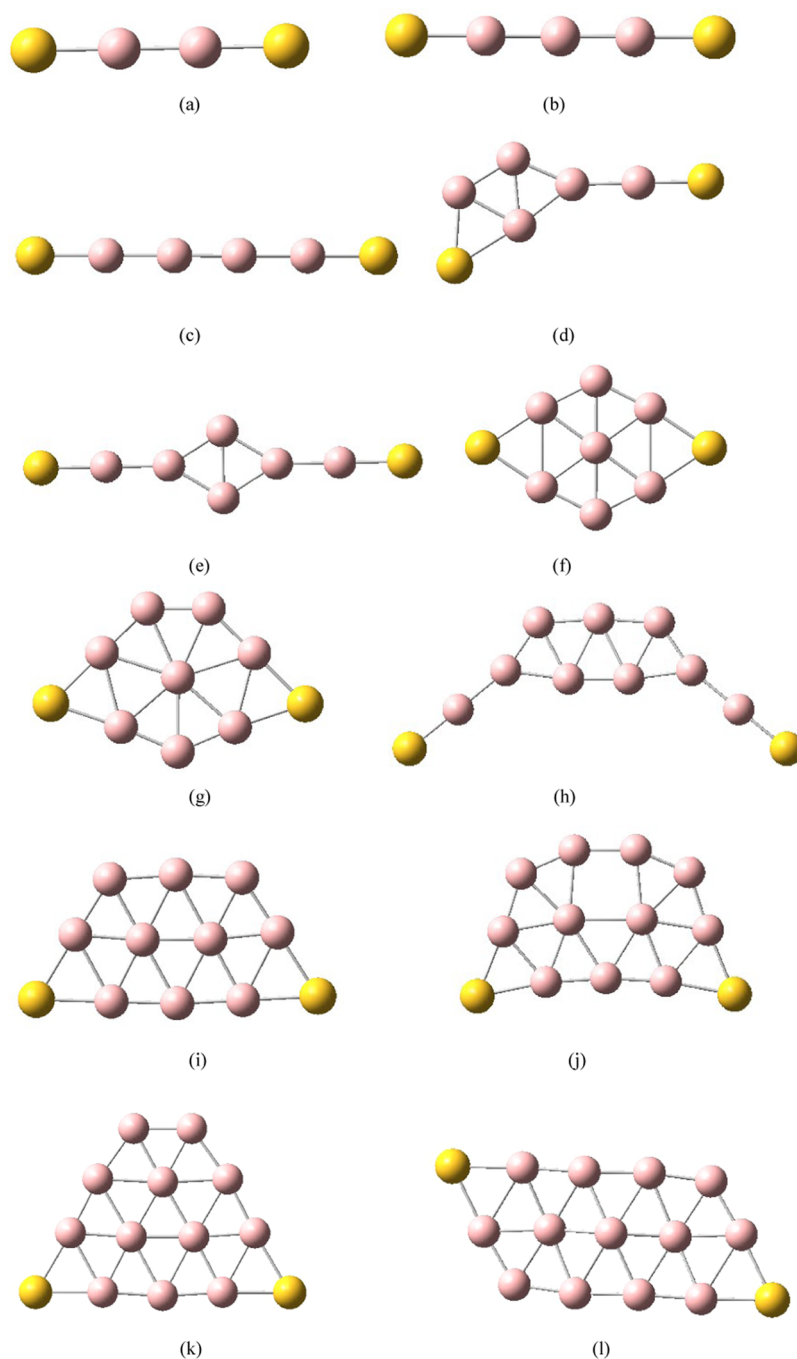
Figure 2. Structures of double S-atom-doped boron clusters $S_2B_n^-$ ($n = 2-13$). (a) $S_2B_2^-$ $D_{\infty h}$; (b) $S_2B_3^-$ $D_{\infty h}$; (c) $S_2B_4^-$ $D_{\infty h}$; (d) $S_2B_5^-$ C_s; (e) $S_2B_6^-$ D_{2h}; (f) $S_2B_7^-$ D_{2h}; (g) $S_2B_8^-$ C_{2h}; (h) $S_2B_9^-$ C_{2v}; (i) $S_2B_{10}^-$ C_{2v}; (j) $S_2B_{11}^-$ C_{2v}; (k) $S_2B_{12}^-$ C_{2v}; and (l) $S_2B_{13}^-$ C_2.

structure,[57] and $BS^{-/0}$ clusters with a B−S triple bond.[58] In particular, the structure evolution of boron clusters after the addition of two nonmetallic atoms was poorly reported. The study of two S atoms of doped boron clusters will fill the vacancy of doped boron clusters in this respect. Similar to B_7, small doped boron clusters are expected to be the structural units of borophene and other boron nanomaterials. Herein, we investigate the effects of two S-atom doping on the structural and electronic properties of boron clusters (B atom $n = 2-13$) using the density functional theory (DFT) method PBE0.[59] Our study aims to provide a detailed understanding of the evolution of the structure and electronic properties of boron clusters upon double S doping. Research of small doped boron

clusters and low-dimensional boron nanostructures is promising to offer new ideas for new nanomaterials and nanodevices.

2. COMPUTATIONAL DETAILS

Geometric structure searches of two S-atom-doped boron clusters $S_2B_n^{0/-}$ ($n = 2-13$) were implemented using particle swarm optimization (CALYPSO) software.[60] CALYPSO is a powerful cluster structure search method, which has been successfully applied to boron and doped boron clusters.[11,25] The PBE0/3-21G level was used for the preliminary structural search. In each generation, 70% of the structures were produced by particle swarm optimization (PSO) operations, while the others were randomly generated. When cluster sizes
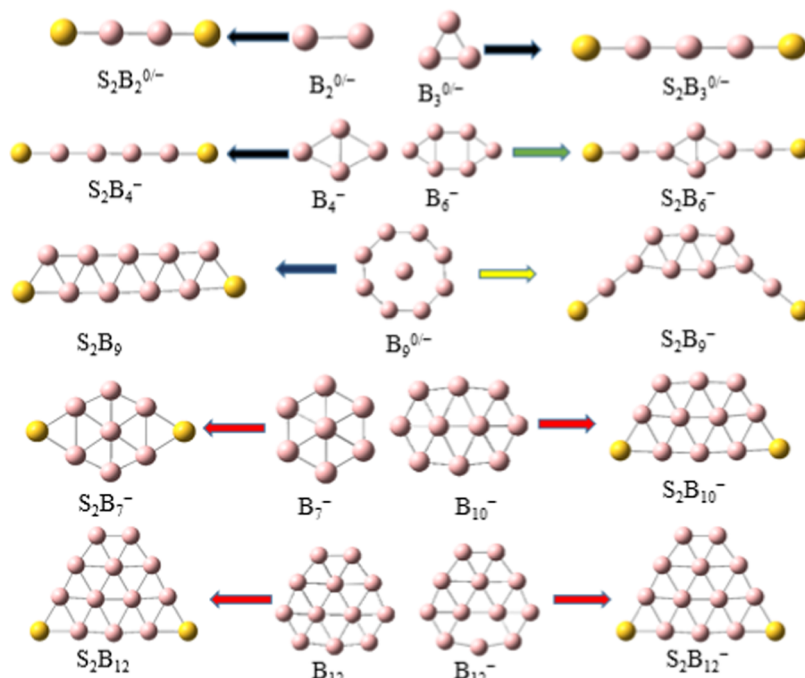
Figure 3. Typical regulation of pure boron clusters by two sulfur atoms. The black arrow shows the adjustment effect of the straight chain structure, the green arrow shows the adjustment effect of the quasi-linear-chain structure, the blue arrow shows the adjustment effect of the double linear-chain structure, the yellow arrow shows the adjustment effect of the single- and double-chain structures, and the red arrow shows the adjustment effect of quasi-planar to perfect planar structures.

vary from $n = 2$ to 9, there were nearly 40−1600 isomers initially obtained for each boron cluster. When cluster sizes vary from $n = 10$ to 13, there were nearly 2000 isomers initially obtained for each boron cluster.

Low-energy structures were then fully optimized at the PBE0/6-311+G* levels.[59,61] After the geometry optimizations, frequency analyses were conducted and electronic structures were studied at the PBE0/6-311+G* level. PBE0/6-311+G(d) are reliable levels for the boron cluster;[12,42,62−65] specifically, theoretical calculation results with the PBE0/6-311+G(d) level agrees with the experimental results.[12] Therefore, the discussion below is on the basis of the PBE0/6-311+G(d) level. All computations were performed using Gaussian 16 software.[66] All analyses and various types of isosurface map drawings were realized using the Multiwfn 3.7 code[67] and VMD.[68]

3. RESULTS AND DISCUSSION

3.1. Structures and Electronic Properties. Five low-energy structures of two sulfur atom-doped boron clusters $S_2B_n^{0/-}$ ($n = 2–13$) are shown in Figures S1−S24, and the lowest energy structures of $S_2B_n^{0/-}$ ($n = 2–13$) are shown in Figures 1 and 2. The calculation results show that the lowest energy structures of $S_2B_n^{0/-}$ ($n = 2–13$) show an evolution from a linear-chain structure to a planar or quasi-planar structure. Early experimental and theoretical works found that most small neutral pure boron clusters are planar or quasi-planar structures, and all small monoanionic boron clusters are planar or quasi-planar structures. After adding two sulfur atoms, the lowest energy structures of S_2B_n ($n = 7, 10–11, 13$) and $S_2B_n^-$ ($n = 13$) have quasi-planar structures; however, the lowest energy structures of S_2B_n ($n = 4–6, 8–9, 12$) and $S_2B_n^-$ ($n = 5–12$) have perfect planar structures. It can be seen from Figures 1 and 2 and the calculation results that after adding

two S atoms, some lowest energy structures of $S_2B_n^{0/-}$ ($n = 2–13$) have a skeleton of pure boron clusters, such as S_2B_n ($n = 4–5, 7, 8, 10–13$) and $S_2B_n^-$ ($n = 7, 8, 10–13$); two S atoms are connected to boron atoms of the pure boron clusters B_n ($n = 4–5, 7–8, 10–13$) and B_n^- ($n = 7–8, 10–13$).[69] However, the addition of two S atoms can modify and improve some of the pure boron cluster structures, and Figure 3 shows the typical regulation of pure boron clusters by two sulfur atoms. Boron is electron-deficient and boron clusters do not form linear chains. As can be seen in Figure 3, two S-atom doping can adjust the pure boron clusters $B_n^{0/-}$ ($n = 2, 3$) and B_4^- to a linear-chain structure and adjust the pure boron clusters B_6^- to a quasi-linear-chain structure. Interestingly, the addition of two sulfur atoms can promote the planarization of quasi-planar pure boron clusters B_7^-, B_{10}^-, and $B_{12}^{0/-}$ and produce perfect planar clusters $S_2B_7^-$, $S_2B_{10}^-$, and $S_2B_{12}^{0/-}$. For $S_2B_7^{0/-}$, $S_2B_{10}^{0/-}$, and $S_2B_{12}^{0/-}$, the lowest energy structures of the neutral cluster and corresponding anionic cluster have similar structures, and two S atoms of S_2B_7 and S_2B_{10} are connected to the pure quasi-planar B_7 and B_{10} clusters, respectively; however, two S atom of $S_2B_7^-$, $S_2B_{10}^-$, and $S_2B_{12}^{0/-}$ are connected to the pure quasi-planar B_7^-, B_{10}^-, and $B_{12}^{0/-}$ clusters, which leads to perfect planar $S_2B_7^-$, $S_2B_{10}^-$, and $S_2B_{12}^{0/-}$, respectively.[69] The lowest energy structures of $S_2B_8^{0/-}$ have similar planar structures, and two S atoms of $S_2B_8^{0/-}$ are connected to the planar $B_8^{0/-}$ clusters. Pure $B_9^{0/-}$ has the same planar wheel-shaped structure;[69] however, doping of two S atoms causes neutral S_2B_9 to become a double-chain planar structure. Doping of two S atoms causes anionic $S_2B_9^-$ to become single- and double-chain planar structures, the upper part of the molecule consists of seven boron atoms forming a double chain, and the lower part of the molecule consists of two B−S binary structures connected to each end of the double chain. The lowest energy structures of S_2B_{10} have

quasi-planar structures and exhibit two axially chiral isomers, and two S atoms of S_2B_{10} are connected to the pure planar B_{10} cluster. The lowest energy structures of $S_2B_{11}^{0/-}$ have a similar structure and two S atoms of $S_2B_{11}^-$ are connected to the pure planar B_{11}^- cluster, which maintains the planar structure; however, two S atoms of S_2B_{11} are connected to the pure planar B_{11} cluster, which leads to the slightly structural change.[69] The lowest energy structures of $S_2B_{12}^{0/-}$ have the same planar structure, and two S atoms are connected to the pure quasi-planar $B_{12}^{0/-}$ cluster, which leads to perfect planar $S_2B_{12}^{0/-}$, respectively. The lowest energy structures of $S_2B_{13}^{0/-}$ have similar quasi-planar structures, and two S atoms of $S_2B_{13}^-$ are connected to the pure quasi-planar B_{13}^- cluster, which leads to a slight structural change.

As can be seen from Figures 1 and 2, two S atoms are located at opposite ends of the molecule, and the distance between the two S atoms is just a measure of the length of the molecule. The distances between two S atoms in the $S_2B_n^{0/-}$ (n = 2−13) clusters are given in Figure 4. Figure 4 shows that the
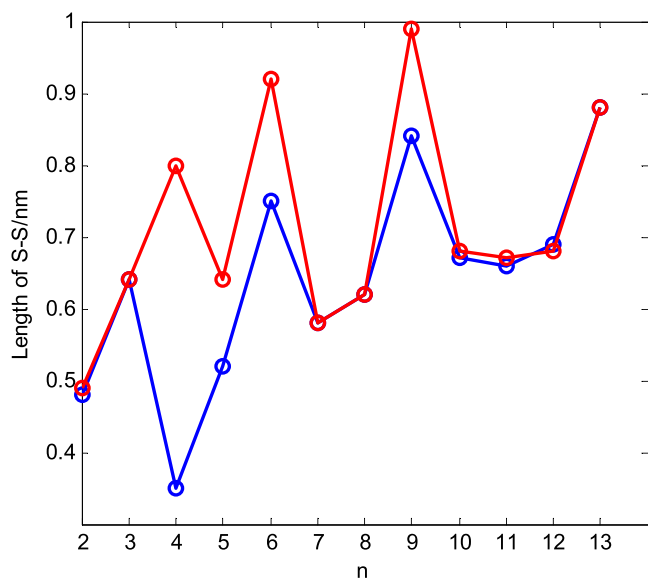
Figure 4. Length of S−S for doped boron clusters $S_2B_n^{0/-}$ (n = 2−13). Blue represents the neutral cluster, red represents the anion cluster, and n represents the number of boron atoms in the cluster.

S−S distances between the neutral and anionic clusters are essentially equal if they have similar structures and that if the neutral and anionic clusters have different structures, the S−S distances of anions are greater than the S−S distances of the corresponding neutral clusters. As can be seen from Figure 4, the S−S distances are mainly in the range of 0.6−1 nm and the two S-atoms are exactly at the two ends of the molecule, which can be used as a bridge connecting gold electrodes in molecular devices, and these clusters are promising for further applications in single-molecule devices. Similar to pure B_7 clusters, planar and quasi-planar S-doped boron clusters are expected to become the basic unit of boron nanomaterials, which will be further synthesized into borophene.

The lowest harmonic frequency analysis confirmed that these lowest energy structures are indeed stable (no imaginary frequency). To further illustrate the relative stability of the clusters $S_2B_n^{0/-}$ (n = 2−13), the average binding energies E_b and second-order energy differences Δ^2E of the clusters are calculated as follows:

$$E_b(S_2B_n) = [nE(B) + 2E(S) - E(S_2B_n)]/(2 + n) \qquad (1)$$

$$E_b(S_2B_n^-) = [(n-1)E(B) + E(B^-) + 2E(S) \\ - E(S_2B_n^-)]/(2 + n) \qquad (2)$$

$$\Delta^2E(S_2B_n^{0/-}) = E(S_2B_{n-1}^{0/-}) + E(S_2B_{n+1}^{0/-}) \\ - 2E(S_2B_n^{0/-}) \qquad (3)$$

where E is the total energy of the atom or cluster *and* n is the number of boron atoms. The calculation results are presented in Figure 5. It can be noted from Figure 5, except for $S_2B_2^{-/0}$,
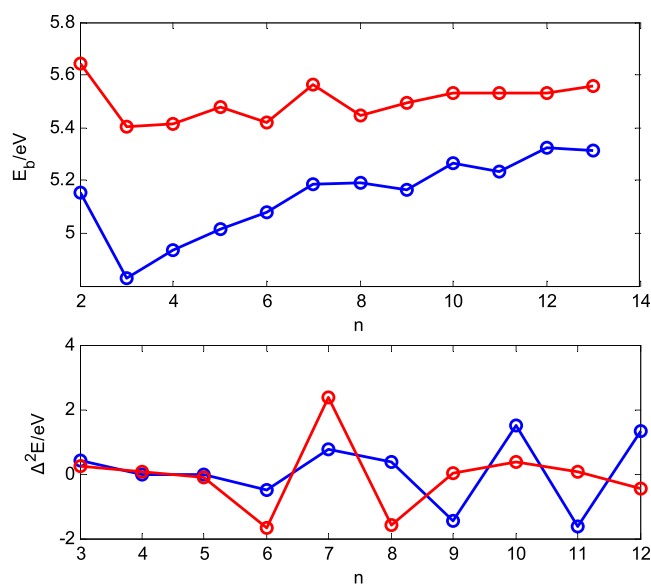
Figure 5. Average binding energy E_b and second-order energy differences Δ^2E of doped boron clusters $S_2B_n^{0/-}$ (n = 2−13). Blue represents the neutral cluster, red represents the anion cluster, and n represents the number of boron atoms in the cluster.

the E_b of $S_2B_n^{-/0}$ (n = 2−13) clusters gradually increase with the increase of n, suggesting that the $S_2B_n^{-/0}$ (n = 3−13) clusters become possibly more and more stable. Furthermore, the E_b for anions is larger than those of the corresponding neutrals, indicating that the anions are more stable and the extra electrons enhance the stabilities of the S-doped boron cluster. $S_2B_2^-$ has the largest average binding energy E_b of 5.63 eV, revealing its superior stability. The second-order difference of Δ^2E is also an important indicator to present the relative stability. The Δ^2E values of the $S_2B_n^{0/-}$ clusters are displayed in Figure 5. It can be seen from Figure 5 that the $S_2B_7^-$, S_2B_{10}, and S_2B_{12} clusters have significantly higher second-order differences than their neighbors, revealing that they are relatively stable compared to the adjacent cluster. The closed shells $S_2B_7^-$, S_2B_{10}, and S_2B_{12} have significantly higher E_b and Δ^2E, indicating their relative stability.

For the closed-shell cluster, the highest occupied molecular orbital (HOMO)−lowest unoccupied molecular orbital (LUMO) energy gaps of S_2B_2, $S_2B_3^-$, S_2B_4, $S_2B_5^-$, S_2B_6, $S_2B_7^-$, S_2B_8, $S_2B_9^-$, S_2B_{10}, $S_2B_{11}^-$, S_2B_{12}, and $S_2B_{13}^-$ are 5.57, 1.37, 3.66, 3.82, 4.26, 3.81, 2.90, 3.47, 2.88, 3.27, 3.2, and 2.63 eV, respectively. For open-shell clusters, α-HOMO−LUMO and β-HOMO−LUMO energy gaps vary within the range of 1.81−5.02 eV. For the closed-shell cluster, the calculated HOMO−LUMO energy gaps reveal that the linear-chain-

2×1c-2e
ON=1.9799 |e|

3×2c-2e σ bonds
ON=1.9950-1.9984|e|

2×2c-2e π bonds
ON=1.9727|e|

2×2c-2e π bonds
ON=1.9727 |e|
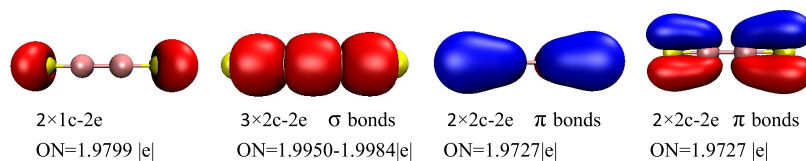
Figure 6. Bonding patterns of S_2B_2. The occupation numbers (ONs) are indicated, and the yellow ball represents the S atom.

2×1c-2e
ON=1.9689 |e|

8×2c-2e σ bonds
ON=1.9286-1.9645|e|

2×3c-2e π bonds
ON=1.9867|e|

2×3c-2e σ bonds
ON=1.8017 |e|

2×4c-2e π bonds
ON=1.9093|e|

1×7c-2e σ bond
ON=1.9751 |e|
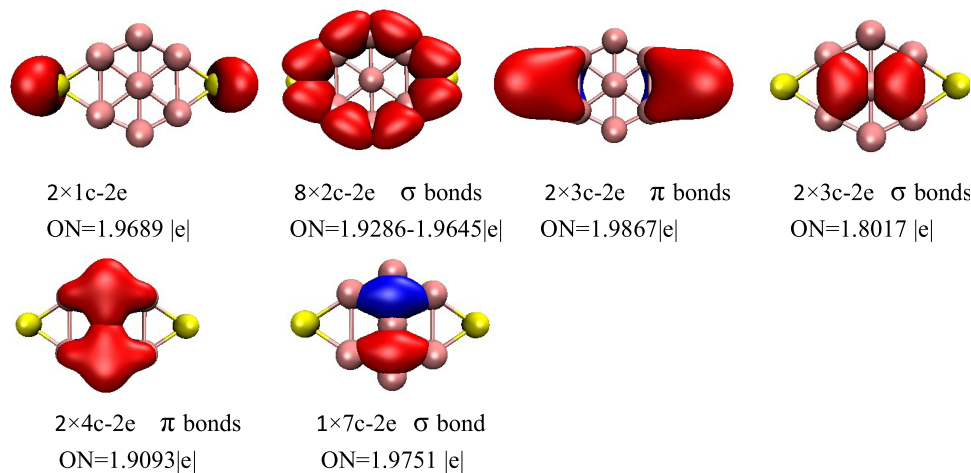
Figure 7. Bonding patterns of $S_2B_7^-$. The occupation numbers (ONs) are indicated, and the yellow ball represents the S atom.

2×1c-2e
ON=1.9595 |e|

10×2c-2e σ bonds
ON=1.8323-1.9560|e|

2×3c-2e π bonds
ON=1.9884|e|

1×3c-2e σ bond
ON=1.8620 |e|

2×4c-2e σ bonds
ON=1.9394|e|

2×4c-2e π bonds
ON=1.8642 |e|

1×5c-2e π bond
ON=1.8424|e|

1×5c-2e σ bond
ON=1.7864|e|
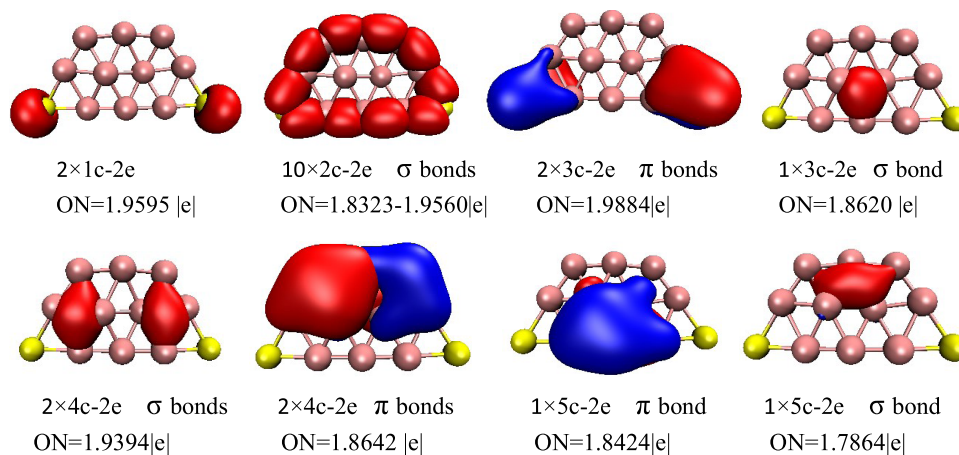
Figure 8. Bonding patterns of S_2B_{10}. The occupation numbers (ONs) are indicated, and the yellow ball represents the S atom.

structure S_2B_2 cluster possesses the largest HOMO−LUMO gap of 5.57 eV and the linear-chain-structure S_2B_3 cluster possesses the smallest HOMO−LUMO gap of 1.37 eV, which show the superior chemical stability of S_2B_2 and the superior chemical activity of $S_2B_3^-$, respectively.

To further understand the stability of $S_2B_n^{0/-}$ ($n = 2-13$), we analyzed the chemical bonding of closed-shell clusters using the adaptive natural density partitioning (AdNDP) approach, which was performed with Multiwfn software. Figures 6−9 and S25−S32 display bonding patterns. For S_2B_2, AdNDP analyses reveal that two lone pairs (see Figure 6) are found on the S atoms and three 2c−2e σ bonds on the adjacent two atoms. The remaining four bonds contain four π bonds, which are distributed symmetrically on B−S atoms at either end of the linear molecule. Overall, the three 2c−2e σ bonds cover the linear molecule, which renders stability to the S_2B_2 cluster, and the 2c−2e π bonds further stabilize the S_2B_2 cluster. For $S_2B_7^-$, AdNDP analyses reveal that two lone pairs (see Figure 7) are

found on the S atoms and eight 2c−2e σ bonds along the peripheral B−B and B−S bonds. The remaining seven bonds contain three σ bonds and four π bonds, which are readily classified into four sets (as shown in Figure 7): two 3c−2e π bonds distributed around the B−S−B triangle at each end of the molecule, two 3c−2e σ bonds distributed around the two B_3 triangles adjacent to the S atoms, two 4c−2e π bonds distributed symmetrically around the two B_4 rings, and one 7c−2e σ bond on the B_7 atoms. Overall, the eight 2c−2e σ bonds, two delocalized 3c−2e σ bonds, and one delocalized 7c−2e σ bond cover the planar molecule, which renders stability to the $S_2B_7^-$ cluster, and the delocalized 3c−2e π bonds and 4c−2e π bonds further stabilizes the $S_2B_7^-$ cluster. As shown in Figure 8, the bonding pattern of S_2B_{10} can be classified into four categories. First, there are two lone pairs on the S atoms. Then, there are ten 2c−2e σ bonds along the peripheral B−B and B−S bonds. Third, one delocalized 3c−2e σ bond, two delocalized 4c−2e σ bonds, and one delocalized

2×1c-2e	11×2c-2e σ bonds	2×2c-2e π bonds	6×3c-2e σ bonds
ON=1.9708 |e|	ON=1.8508-1.9549|e|	ON=1.7757|e|	ON=1.7653 |e|

2×5c-2e π bonds	1×6c-2e π bond
ON=1.8077-1.8359|e|	ON=1.7411 |e|
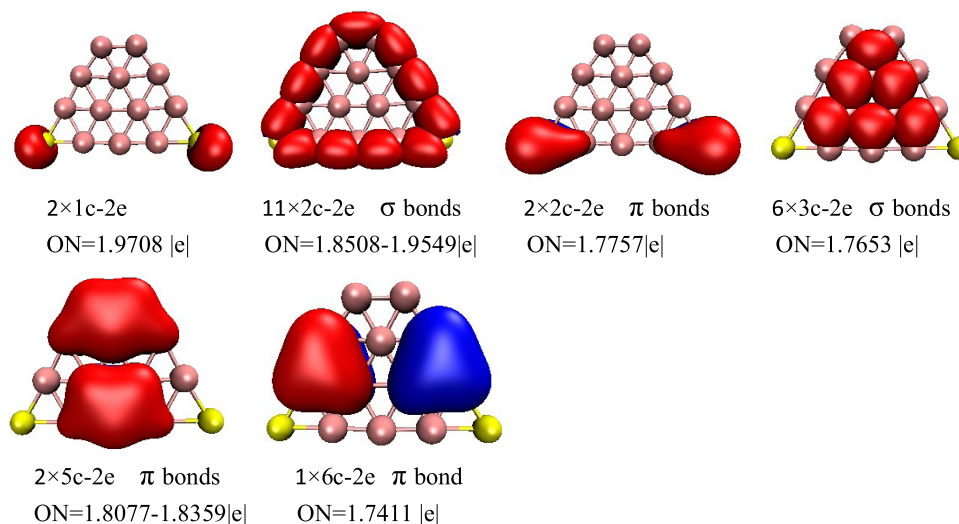
Figure 9. Bonding patterns of S_2B_{12}. The occupation numbers (ONs) are indicated, and the yellow ball represents the S atom.

5c−2e σ bond cover the inner region of the B_{10} construction, which renders stability to the S_2B_{10} cluster. Finally, two delocalized 3c−2e π bonds, two delocalized 4c−2e π bonds, and one delocalized 5c−2e π bond cover the entire molecular surface, which enhances the stability of S_2B_{10}. Figure 9 displays the bonding patterns of planar S_2B_{12}. The bonding pattern of S_2B_{12} can be classified into three categories. First, there are two lone pairs on the S atoms. Then, there are 11 2c−2e σ bonds that fill with the peripheral ring and six delocalized 3c−2e σ bonds that cover the inner region of the B_{12} construction, which renders stability to the S_2B_{12} cluster. Finally, two delocalized 2c−2e π bonds, two delocalized 5c−2e π bonds, and one delocalized 6c−2e π bond cover the entire molecular surface, which enhances the stability of S_2B_{12}. As shown in Figures S25−S32, all clusters have two lone pairs, different numbers of 2c−2e σ bonds and 2c−2e π bonds, and different numbers of delocalized π bonds and σ bonds, which play important roles in their stability. These delocalized π and σ bonds indicate that the delocalized electron clouds are distributed almost evenly on each part of the molecule and effectively reduce the intramolecular electrostatic repulsion to some extent in the system, which plays a prominent role in their stability.

AdNDP bonding analyses revealed that the linear-chain-structure S_2B_3 and planar $S_2B_{11}^-$ clusters possess five π bonds, which quite surprisingly follow the 4m + 2 Hückel rule for π aromaticity; however, linear-chain-structure S_2B_3 and planar SeB_{11}^- clusters possess 4 σ bonds and 16 σ bonds, respectively, which quite surprisingly follow the 4m Hückel rule for σ antiaromaticity. Furthermore, the linear-chain-structure S_2B_2, planar S_2B_6, and planar $S_2B_7^-$ clusters possess four π bonds, which quite surprisingly follow the 4m Hückel rule for π antiaromaticity; however, the linear-chain-structure S_2B_2 and planar S_2B_6 and $S_2B_7^-$ clusters possess 3 σ bonds, 9 σ bonds, and 11 σ bonds, respectively, which quite surprisingly follow the 4m + 2 Hückel rule for σ aromaticity. Third, the planar $S_2B_5^-$, S_2B_8, $S_2B_9^-$, and $S_2B_{13}^-$ clusters possess 4 π bonds, 4 π bonds, 6 π bonds, and 6 π bonds, respectively, the planar $S_2B_5^-$, S_2B_8, $S_2B_9^-$, and $S_2B_{13}^-$ clusters possess 8 σ bonds, 12 σ bonds, 12 σ bonds, and 18 σ bonds, respectively, which quite surprisingly follow the 4m Hückel rule for π and σ antiaromaticity. Finally, the planar S_2B_4, S_2B_{10}, and S_2B_{12}

clusters possess 3 π bonds, 4 π bonds, and 5 π bonds, respectively, and the planar S_2B_4, S_2B_{10}, and S_2B_{12} clusters possess 7 σ bonds, 13 σ bonds, and 17 σ bonds, respectively, which quite surprisingly follow the 4m + 2 Hückel rule for π and σ aromaticity. S_2B_4, S_2B_{10}, and S_2B_{12} have a skeleton of pure boron clusters and pure boron clusters B_4, B_{10}, and B_{12} are doubly (π and σ) aromatic systems.[69] The addition of two S atoms maintains the doubly (π and σ) aromatic system. In particular, the addition of two S atoms leads to the evolution of quasi-planar B_{12} into a perfect planar structure, which also maintains the characteristics of doubly (π and σ) aromaticity.

To further characterize the electron localization and chemical bonds. The electron localization function (ELF)[70] of the valence electrons was analyzed, as shown in Figures S33−S35. ELF can well describe the delocalization of electrons. When the isosurface value is 0.60, the isosurface maps of $S_2B_2^-$, S_2B_4, S_2B_5, $S_2B_7^{0/-}$, $S_2B_8^{0/-}$, S_2B_9, $S_2B_{10}^{0/-}$, $S_2B_{12}^{0/-}$, and $S_2B_{13}^{0/-}$ are connected on the surface of the whole molecule. Among these clusters, the isosurface maps of $S_2B_7^{0/-}$, $S_2B_8^{0/-}$, and $S_2B_{13}^{0/-}$ are not connected in some places, indicating that the delocalization of the whole molecule is a little weaker than that of other clusters ($S_2B_2^-$, S_2B_4, S_2B_5, S_2B_9, $S_2B_{10}^{0/-}$, and $S_2B_{12}^{0/-}$). On the other hand, the isosurface diagrams of S_2B_2, $S_2B_3^{0/-}$, $S_2B_4^-$, $S_2B_5^-$, $S_2B_6^{0/-}$, $S_2B_9^-$, and $S_2B_{11}^{0/-}$ are disconnected on the surface of the whole molecule, indicating that the delocalization of the whole molecule is weaker than that of the other clusters. Figure S34 shows the ELF when the isosurface value is 0.70. With this isosurface value, the isosurface diagram of all clusters is disconnected on the surface of the whole molecule, while the isosurface diagrams of some clusters are still connected on the partial region of the molecule, indicating that different delocalization characteristics of these clusters. Figure S35 shows the ELF when the isosurface value is 0.80. Under this isosurface value, the isosurface maps of some clusters are disconnected and there are no connected regions. However, the isosurface maps of some clusters show that there is still some connected area on the surface of the molecule, indicating that the local delocalization of these clusters is stronger than that of other clusters. ELF analyses further confirm these comments based on the AdNDP analyses, such as the contributions from valence electrons of S_2B_2 partitioned in
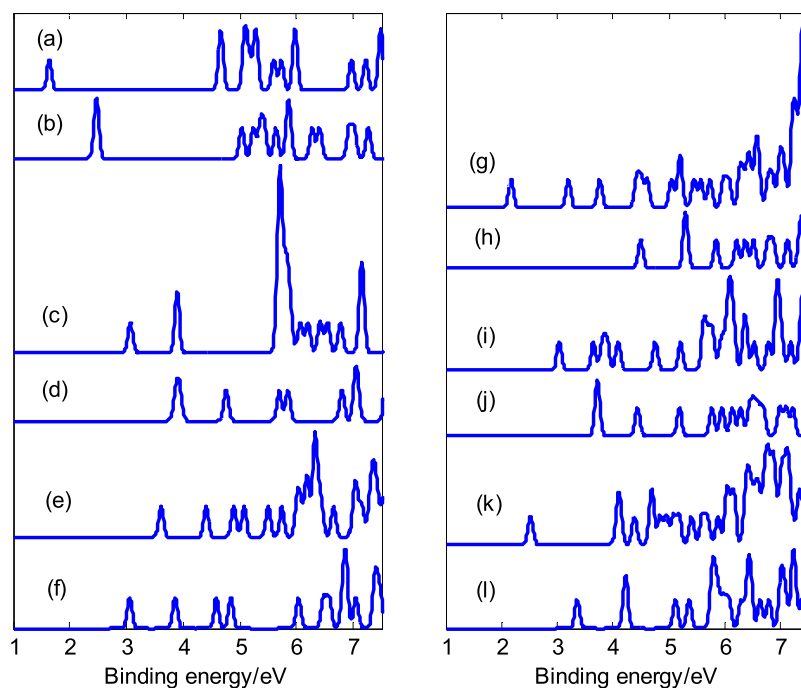
Figure 10. Calculated photoelectron spectra with the PBE0/6-311+G* method. (a) $S_2B_2^-$, (b) $S_2B_3^-$, (c) $S_2B_4^-$, (d) $S_2B_5^-$, (e) $S_2B_6^-$, (f) $S_2B_7^-$, (g) $S_2B_8^-$, (h) $S_2B_9^-$, (i) $S_2B_{10}^-$, (j) $S_2B_{11}^-$, (k) $S_2B_{12}^-$, and (l) $S_2B_{13}^-$. The simulations were done by fitting the distributions of calculated vertical detachment energies at the PBE0 level with unit-area Gaussian functions of 0.05 eV half-width.

Figure 6. Isosurface maps of S_2B_2 (Figure S33) cover the B−S bonds at both ends of the linear-chain molecule that correspond to two 2c−2e σ bonds and four orthogonal 2c−2e π bonds. The smaller isosurface maps of the B−B bond in the middle of the linear-chain molecule corresponds to the 2c−2e B−B σ bond. Isosurface maps on the B−S bonds at both ends of the linear-chain molecule are fatter due to another four 2c−2e π bonds. Similarly, isosurface maps of $S_2B_3^-$ (Figure S33) cover the B−S bonds at both ends of the linear-chain molecule that correspond to two 2c−2e σ bonds and four orthogonal 2c−2e π bonds (Figure S25). The isosurface maps of the B−B−B bond in the middle of the linear-chain molecule correspond to two 2c−2e B−B σ bonds and one 3c−2e B−B−B π bond (Figure S25). The isosurface maps of the B−B−B bond in the paper direction is fatter than the isosurface maps perpendicular to the paper direction due to the 3c−2e B−B−B π bond in the paper direction. Considering the electron delocalization characteristics of these clusters, they are expected to be applied to molecular devices.

Figure S36 shows the isosurface diagram of the spin density of open-shell clusters. Spin density reveals the distribution of unpaired electrons (single electrons) in three-dimensional space. A positive spin density means that there are more α electrons than β electrons, while a negative spin density means that there are more β electrons than α electrons. Figure S36 shows a spin density diagram for an isosurface value of 0.002. Green represents a positive value (α electrons), while blue represents a negative value (β electrons). It can be seen from Figure S36 that the unpaired single electrons are mostly α electrons, and there are a small number of β electrons distributed on B atoms. For open-shell clusters ($S_2B_2^-$, S_2B_3, $S_2B_4^-$, $S_2B_8^-$, S_2B_{11}, and $S_2B_{12}^-$), the unpaired electrons are almost all α electrons. For open-shell clusters ($S_2B_6^-$, $S_2B_7^-$, $S_2B_{12}^-$, and S_2B_{13}), most of the unpaired electrons are distributed on the B atom; there are no unpaired electrons

on the S atom. For open-shell clusters (S_2B_5, $S_2B_8^-$, S_2B_9, $S_2B_{10}^-$ and S_2B_{11}), most of the unpaired electrons are distributed on the B atom, and only a small part of the unpaired electrons is on S atoms. As shown in Figure S36, the unpaired single electrons of $S_2B_2^-$, S_2B_3, $S_2B_4^-$, S_2B_7, $S_2B_8^-$, $S_2B_{12}^-$, and S_2B_{13} have π electron characteristics, and the unpaired single electrons of S_2B_5, $S_2B_6^-$, S_2B_9, $S_2B_{10}^-$, and S_2B_{11} have σ characteristics. These spin features are expected to produce interesting magnetic properties, which will further lead to potential applications in molecular devices. In addition, the spin density reflects chemical reactions or adsorption to a certain extent. The single electrons of these clusters are mostly α electrons. The B or S atoms containing α single electrons can pair with free radicals or small molecules containing β single electrons to form new covalent bonds, while B atoms with single β electrons can adsorb or react with atoms, free radicals, or small molecules with α single electrons.

3.2. Photoelectron Spectra. Photoelectron spectroscopy, in combination with theoretical calculations, has been used to understand and identify the structures of size-selected boron clusters.[3,12,71] To facilitate future identifications of $S_2B_n^-$ ($n = 2−13$), we calculated the vertical detachment energies (VDEs) and simulated the photoelectron spectra for $S_2B_n^-$ ($n = 2−13$) with the time-dependent DFT (TD-DFT) method.[12,71,72]

Figure 10 presents the photoelectron spectra of $S_2B_n^-$ ($n = 2−13$). The predicted photoelectron spectra show that $S_2B_2^-$ has the lowest first VDE and the largest energy gap (about 3 eV) between the first and second bands. The first several bands of photoelectron spectra were used to identify boron clusters,[3,12] so we will focus on the bands at the low binding energy side. The first peaks of these photoelectron spectra (except for $S_2B_3^-$, $S_2B_5^-$, $S_2B_{11}^-$) come from the calculated ground-state VDEs of $S_2B_2^-$, $S_2B_4^-$, $S_2B_6^-$, $S_2B_7^-$, $S_2B_8^-$, $S_2B_9^-$, $S_2B_{10}^-$, $S_2B_{12}^-$, and $S_2B_{13}^-$ at 1.64, 3.06, 3.61, 3.06, 2.17, 4.49, 3.03, 2.52, and 3.35 eV, respectively. The calculated ground-

state VDEs of these closed-shell clusters ($S_2B_7^-$, $S_2B_9^-$, and $S_2B_{13}^-$) originate from the detachment of the electron from the molecular orbital (HOMO). For open-shell clusters ($S_2B_2^-$, $S_2B_6^-$, $S_2B_8^-$, $S_2B_{10}^-$, and $S_2B_{12}^-$), the calculated ground-state VDE of each cluster originates from the detachment of the electron from the molecular orbital α-HOMO; however, for open-shell clusters $S_2B_4^-$, the calculated ground-state VDE originates from the detachment of the electron from molecular orbital β-HOMO. The first peak of $S_2B_3^-$ comes from the ground state and the second VDE at 2.46 and 2.47 eV, respectively. The first peaks of $S_2B_n^-$ (n = 5, 11) come from the ground-state and second VDEs at 3.94 and 3.87 eV for $S_2B_5^-$ 3.72 and 3.71 eV for $S_2B_{11}^-$, respectively, in which the second VDE is smaller than the ground-state VDE. The second peak of $S_2B_7^-$ comes from the second calculated VDEs at 3.85 eV, which originate from detaching the electrons from HOMO—1. The second peaks of $S_2B_3^-$, $S_2B_5^-$, and $S_2B_{11}^-$ come from the third calculated VDEs at 5.03, 4.76, and 4.43 eV, respectively, which originate from detaching the electrons from HOMO—2. The second peaks of SeB_6^- and SeB_8^- come from the second VDEs at 4.40 and 3.20 eV, respectively, which originate from detaching the electrons from the molecular orbital β-HOMO. The second peak of $S_2B_{10}^-$ comes from the third simulated VDEs at 3.64 eV. The second peaks of $S_2B_n^-$ (n = 2, 4, 9, 12, 13) come from the second and third simulated VDEs at 4.66 and 4.67 eV for $S_2B_2^-$, 3.88 and 3.89 eV for $S_2B_4^-$, 5.28 and 5.30 eV for $S_2B_9^-$, 4.08 and 4.11 eV for $S_2B_{12}^-$, and 4.20 and 4.23 eV for $S_2B_{13}^-$, respectively. In addition, the peaks with higher binding energy originate from detaching the electrons from lower molecular orbitals.

It is noted that some of the doped anionic boron clusters have similar skeletons to the corresponding anionic pure boron clusters. Comparing their photoelectron spectra, the addition of two S atoms results in a change in the photoelectron spectra of some doped boron clusters. However, the photoelectron spectra of some doped boron clusters are similar to that of the corresponding anionic pure boron clusters. For example, compared with the photoelectron spectra of pure boron cluster B_7^-, the addition of two S atoms causes the first peak of $S_2B_7^-$ to move 0.20 eV toward the high binding energy side and causes the second peak of $S_2B_7^-$ to move 0.40 eV toward the high binding energy side. Similarly, compared with the photoelectron spectra of pure boron clusters B_{11}^- and B_{13}^-, the addition of two S atoms causes the first and second peaks of $S_2B_{11}^-$ and $S_2B_{13}^-$ to move 0.22−0.34 eV toward the high binding energy side.[69] For $S_2B_8^-$, compared with the photoelectron spectra of the pure boron cluster B_8^-, the addition of two S atoms causes different spectral features. Comparing with the photoelectron spectra of the pure boron cluster B_{10}^-, planar $S_2B_{10}^-$ and quasi-planar B_{10}^- have almost the same first two VDEs (3.03 and 3.64 eV for $S_2B_{10}^-$, 3.06 ± 0.03 and 3.61 ± 0.04 eV for B_{10}^-).[69] For $S_2B_{12}^-$, compared with the photoelectron spectra of pure boron clusters B_{12}^-, the addition of two S atoms causes the first peak to move 0.25 eV toward the high binding energy side and causes the second peak to move 0.23 eV toward the low binding energy side. Figure 10 indicates that $S_2B_n^-$ (n = 2−13) has different spectral features, especially because they have different spectral bands at the low binding energy side. These features can be used to identify the $S_2B_n^-$ (n = 2−13) and provide important information for the identification of $S_2B_n^-$ (n = 2−13).

4. CONCLUSIONS

In this work, density functional theory combined with particle swarm optimization algorithm (CALYPSO) software is used to research the structural evolution of $S_2B_n^{0/-}$ (n = 2−13) clusters. Research results include the following points: (1) The global minima obtained for the $S_2B_n^{0/-}$ (n = 2−13) clusters show an evolution from the linear-chain structure to planar or quasi-planar structures. (2) S_2B_2, $S_2B_2^-$, S_2B_3, $S_2B_3^-$, and $S_2B_4^-$ are linear-chain structures, $S_2B_6^-$ is quasi-linear-chain structures, S_2B_6 and $S_2B_9^-$ are single- and double-chain structures, S_2B_5 and S_2B_9 are double-chain structures. (3) Two S-atom doping can adjust the quasi-planar pure boron clusters (B_7^-, B_{10}^-, and $B_{12}^{0/-}$) to the perfect planar structure. (4) AdNDP bonding analyses revealed that linear S_2B_3 and planar $S_2B_{11}^-$ are π aromaticity and σ antiaromaticity, S_2B_2, planar $S_2B_6^-$, and planar $S_2B_7^-$ clusters are π antiaromaticity and σ aromaticity. Furthermore, AdNDP bonding analyses revealed that S_2B_4, S_2B_{10}, and S_2B_{12} clusters are doubly aromatic, whereas $S_2B_5^-$, S_2B_8, $S_2B_9^-$, and $S_2B_{13}^-$ clusters are doubly antiaromatic. (5) The ELF analysis shows that $S_2B_n^{0/-}$ (n = 2−13) clusters have different electron delocalization characteristics, and the spin density analysis shows that the open-shell clusters have different characteristics of electron spin distribution; the S−S distances of these clusters are mainly in the range of 0.6−1 nm and the two S-atoms are exactly at the two ends of the molecule, which can be used as a bridge connecting gold electrodes in molecular devices. These electronic and geometric properties are promising to provide valuable information for applications in single-molecule devices. (6) Photoelectron spectra of $S_2B_n^-$ (n = 2−13) have different spectral bands at the low binding energy side that can be compared with future experimental values. This research has enriched the structure of nonmetallic atoms in doped boron clusters.

■ ASSOCIATED CONTENT

Ⓢ Supporting Information

The Supporting Information is available free of charge at https://pubs.acs.org/doi/10.1021/acsomega.3c04967.

> Different isomers of $S_2B_n^{0/-}$ (n = 2−13), bonding patterns of closed-shell clusters, electron localization function (ELF) of $S_2B_n^{0/-}$ (n = 2−13), and spin density of open-shell clusters (PDF)

■ AUTHOR INFORMATION

Corresponding Author

Shi-Xiong Li − *School of Physics and Electronic Science, Guizhou Education University, Guiyang 550018, China;* ⓞ orcid.org/0000-0003-2831-5955; Email: leesxoptics@163.com

Authors

Yue-Ju Yang − *School of Physics and Electronic Science, Guizhou Education University, Guiyang 550018, China*
De-Liang Chen − *School of Physics and Electronic Science, Guizhou Education University, Guiyang 550018, China*

Complete contact information is available at:
https://pubs.acs.org/10.1021/acsomega.3c04967

Notes

The authors declare no competing financial interest.

REFERENCES

(1) Boustani, I. Systematic ab initio investigation of bare boron clusters:mDetermination of the geometryand electronic structures of Bn(n = 2−14). *Phys. Rev. B* **1997**, *55*, 16426−16438.

(2) Zhai, H.-J.; Wang, L.-S.; Alexandrova, A. N.; Boldyrev, A. I. Electronic structure and chemical bonding of B_5^- and B_5 by photoelectron spectroscopy andab initiocalculations. *J. Chem. Phys.* **2002**, *117*, 7917−7924.

(3) Zhai, H. J.; Kiran, B.; Li, J.; Wang, L. S. Hydrocarbon analogues of boron clusters–planarity, aromaticity and antiaromaticity. *Nat. Mater.* **2003**, *2*, 827−833.

(4) Kiran, B.; Bulusu, S.; Zhai, H. J.; Yoo, S.; Zeng, X. C.; Wang, L. S. Planar-to-tubular structural transition in boron clusters: B_{20} as the embryo of single-walled boron nanotubes. *Proc. Natl. Acad. Sci. U.S.A.* **2005**, *102*, 961−964.

(5) Bean, D. E.; Fowler, P. W. Double Aromaticity in "Boron Toroids". *J. Phys. Chem. C* **2009**, *113*, 15569−15575.

(6) Chen, Q.; Wei, G. F.; Tian, W. J.; Bai, H.; Liu, Z. P.; Zhai, H. J.; Li, S. D. Quasi-planar aromatic B_{36} and B_{36}^- clusters: all-boron analogues of coronene. *Phys. Chem. Chem. Phys.* **2014**, *16*, 18282−18287.

(7) Sergeeva, A. P.; Popov, I. A.; Piazza, Z. A.; Li, W. L.; Romanescu, C.; Wang, L. S.; Boldyrev, A. I. Understanding boron through size-selected clusters: structure, chemical bonding, and fluxionality. *Acc. Chem. Res.* **2014**, *47*, 1349−1358.

(8) Jian, T.; Chen, X.; Li, S. D.; Boldyrev, A. I.; Li, J.; Wang, L. S. Probing the structures and bonding of size-selected boron and doped-boron clusters. *Chem. Soc. Rev.* **2019**, *48*, 3550−3591.

(9) Casillas, R.; Baruah, T.; Zope, R. R. Geometry and electronic structure of neutral and charged B21 clusters. *Chem. Phys. Lett.* **2013**, *557*, 15−18.

(10) Pham, H. T.; Duong, L. V.; Pham, B. Q.; Nguyen, M. T. The 2D-to-3D geometry hopping in small boron clusters: The charge effect. *Chem. Phys. Lett.* **2013**, *577*, 32−37.

(11) Lv, J.; Wang, Y.; Zhu, L.; Ma, Y. B_{38}: an all-boron fullerene analogue. *Nanoscale* **2014**, *6*, 11692−11696.

(12) Zhai, H. J.; Zhao, Y. F.; Li, W. L.; Chen, Q.; Bai, H.; Hu, H. S.; Piazza, Z. A.; Tian, W. J.; Lu, H. G.; Wu, Y. B.; Mu, Y. W.; Wei, G. F.; Liu, Z. P.; Li, J.; Li, S. D.; Wang, L. S. Observation of an all-boron fullerene. *Nat. Chem.* **2014**, *6*, 727−731.

(13) Bai, H.; Chen, Q.; Zhai, H. J.; Li, S. D. Endohedral and exohedral metalloborospherenes: $M@B_{40}$ (M = Ca, Sr) and $M\&B_{40}$ (M = Be, Mg). *Angew. Chem., Int. Ed.* **2015**, *54*, 941−945.

(14) Li, S.-X.; Zhang, Z.-P.; Long, Z.-W.; Qin, S.-J. Structures, stabilities and spectral properties of metalloborospherenes $MB_{40}^{0/−}$ (M = Cu, Ag, and Au). *RSC Adv.* **2017**, *7*, 38526−38537.

(15) Dong, H.; Hou, T.; Lee, S. T.; Li, Y. New Ti-decorated B_{40} fullerene as a promising hydrogen storage material. *Sci. Rep.* **2015**, *5*, No. 9952.

(16) An, Y.; Zhang, M.; Wu, D.; Fu, Z.; Wang, T.; Xia, C. Electronic transport properties of the first all-boron fullerene B_{40} and its metallofullerene $Sr@B_{40}$. *Phys. Chem. Chem. Phys.* **2016**, *18*, 12024−12028.

(17) Bai, H.; Bai, B.; Zhang, L.; Huang, W.; Mu, Y. W.; Zhai, H. J.; Li, S. D. Lithium-Decorated Borospherene B_{40}: A Promising Hydrogen Storage Medium. *Sci. Rep.* **2016**, *6*, No. 35518.

(18) Shakerzadeh, E.; Biglari, Z.; Tahmasebi, E. $M@B_{40}$ (M = Li, Na, K) serving as a potential promising novel NLO nanomaterial. *Chem. Phys. Lett.* **2016**, *654*, 76−80.

(19) Tang, C.; Zhang, X. The hydrogen storage capacity of Sc atoms decorated porous boron fullerene B_{40}: A DFT study. *Int. J. Hydrogen Energy* **2016**, *41*, 16992−16999.

(20) Li, S.; Zhang, Z.; Long, Z.; Chen, D. Structures, Stabilities, and Spectral Properties of Endohedral Borospherenes $M@B_{40}^{0/−}$ (M = H_2, HF, and H_2O). *ACS Omega* **2019**, *4*, 5705−5713.

(21) Li, S. X.; Zhang, Z. P.; Long, Z. W.; Chen, D. L. Structures, Electronic, and Spectral Properties of Doped Boron Clusters $MB_{12}^{0/−}$ (M = Li, Na, and K). *ACS Omega* **2020**, *5*, 20525−20534.

(22) Mannix, A. J.; Zhou, X. F.; Kiraly, B.; Wood, J. D.; Alducin, D.; Myers, B. D.; Liu, X.; Fisher, B. L.; Santiago, U.; Guest, J. R.; Yacaman, M. J.; Ponce, A.; Oganov, A. R.; Hersam, M. C.; Guisinger, N. P. Synthesis of borophenes: Anisotropic, two-dimensional boron polymorphs. *Science* **2015**, *350*, 1513−1516.

(23) Li, Q.; Kolluru, V. S. C.; Rahn, M. S.; Schwenker, E.; Li, S.; Hennig, R. G.; Darancet, P.; Chan, M. K. Y.; Hersam, M. C. Synthesis of borophane polymorphs through hydrogenation of borophene. *Science* **2021**, *371*, 1143−1148.

(24) Popov, I. A.; Li, W. L.; Piazza, Z. A.; Boldyrev, A. I.; Wang, L. S. Complexes between planar boron clusters and transition metals: a photoelectron spectroscopy and ab initio study of CoB_{12}^- and RhB12(-). *J. Phys. Chem. A* **2014**, *118*, 8098−8105.

(25) Liang, W. Y.; Das, A.; Dong, X.; Cui, Z. H. Lithium doped tubular structure in LiB_{20} and LiB_{20}^-: a viable global minimum. *Phys. Chem. Chem. Phys.* **2018**, *20*, 16202−16208.

(26) Wang, W.; Guo, Y.-D.; Yan, X.-H. The spin-dependent transport of transition metal encapsulated B_{40} fullerene. *RSC Adv.* **2016**, *6*, 40155−40161.

(27) Saha, R.; Kar, S.; Pan, S.; Martinez-Guajardo, G.; Merino, G.; Chattaraj, P. K. A Spinning Umbrella: Carbon Monoxide and Dinitrogen Bound MB_{12}^- (M = Co, Rh, Ir) Clusters. *J. Phys. Chem. A* **2017**, *121*, 2971−2979.

(28) Li, S.-X.; Chen, D.-L.; Zhang, Z.-P.; Long, Z.-W. Ground state structures and properties of Be atom doped boron clusters BeBn(n = 10-15). *Acta Phys. Sin.* **2020**, *69*, No. 193101.

(29) Cheung, L. F.; Kocheril, G. S.; Czekner, J.; Wang, L. S. Observation of Mobius Aromatic Planar Metallaborocycles. *J. Am. Chem. Soc.* **2020**, *142*, 3356−3360.

(30) Popov, I. A.; Jian, T.; Lopez, G. V.; Boldyrev, A. I.; Wang, L. S. Cobalt-centred boron molecular drums with the highest coordination number in the CoB_{16}^- cluster. *Nat. Commun.* **2015**, *6*, No. 8654.

(31) Jian, T.; Li, W. L.; Popov, I. A.; Lopez, G. V.; Chen, X.; Boldyrev, A. I.; Li, J.; Wang, L. S. Manganese-centered tubular boron cluster - MnB_{16}^-: A new class of transition-metal molecules. *J. Chem. Phys.* **2016**, *144*, No. 154310.

(32) Chen, T. T.; Li, W. L.; Bai, H.; Chen, W. J.; Dong, X. R.; Li, J.; Wang, L. S. ReB_8^- and ReB_9^-: New Members of the Transition-Metal-Centered Borometallic Molecular Wheel Family. *J. Phys. Chem. A* **2019**, *123*, 5317−5324.

(33) Cheung, L. F.; Czekner, J.; Kocheril, G. S.; Wang, L. S. ReB_6^-: A Metallaboron Analog of Metallabenzenes. *J. Am. Chem. Soc.* **2019**, *141*, 17854−17860.

(34) Chen, T. T.; Li, W. L.; Chen, W. J.; Yu, X. H.; Dong, X. R.; Li, J.; Wang, L. S. Spherical trihedral metallo-borospherenes. *Nat. Commun.* **2020**, *11*, No. 2766.

(35) Cheung, L. F.; Kocheril, G. S.; Czekner, J.; Wang, L. S. MnB6(-): An Open-Shell Metallaboron Analog of 3d Metallabenzenes. *J. Phys. Chem. A* **2020**, *124*, 2820−2825.

(36) Chen, W. J.; Kulichenko, M.; Choi, H. W.; Cavanagh, J.; Yuan, D. F.; Boldyrev, A. I.; Wang, L. S. Photoelectron Spectroscopy of Size-Selected Bismuth-Boron Clusters: BiBn⁻ (n = 6-8). *J. Phys. Chem. A* **2021**, *125*, 6751−6760.

(37) Jiang, Z. Y.; Chen, T. T.; Chen, W. J.; Li, W. L.; Li, J.; Wang, L. S. Expanded Inverse-Sandwich Complexes of Lanthanum Borides: $La_2B_{10}^-$ and $La_2B_{11}^-$. *J. Phys. Chem. A* **2021**, *125*, 2622−2630.

(38) Barroso, J.; Pan, S.; Merino, G. Structural transformations in boron clusters induced by metal doping. *Chem. Soc. Rev.* **2022**, *51*, 1098−1123.

(39) Đorđević, S.; Radenkovic, S. Spatial and Electronic Structures of BeB$_8$ and MgB$_8$: How far Does the Analogy Go? *ChemPhysChem* **2022**, *23*, No. e202200070.

(40) Chacko, S.; Kanhere, D. G.; Boustani, I. Ab initiodensity functional investigation of B$_{24}$ clusters: Rings, tubes, planes, and cages. *Phys. Rev. B* **2003**, *68*, No. 035414.

(41) Liang, W.-y.; Das, A.; Dong, X.; Wang, M.-h.; Cui, Z.-h. Structural and electronic properties of MB$_{22}^-$ (M = Na, K) clusters: tubular boron versus quasi-planar boron forms. *New J. Chem.* **2019**, *43*, 6507−6512.

(42) Chen, B. L.; Sun, W. G.; Kuang, X. Y.; Lu, C.; Xia, X. X.; Shi, H. X.; Maroulis, G. Structural Stability and Evolution of Medium-Sized Tantalum-Doped Boron Clusters: A Half-Sandwich-Structured TaB12(-) Cluster. *Inorg. Chem.* **2018**, *57*, 343−350.

(43) Lv, J.; Wang, Y.; Zhang, L.; Lin, H.; Zhao, J.; Ma, Y. Stabilization of fullerene-like boron cages by transition metal encapsulation. *Nanoscale* **2015**, *7*, 10482−10489.

(44) Yang, Y. J.; Li, S. X.; Chen, D. L.; Long, Z. W. Structural and Electronic Properties of Single-Atom Transition Metal-Doped Boron Clusters MB$_{24}$ (M = Sc, V, and Mn). *ACS Omega* **2021**, *6*, 30442−30450.

(45) Li, S. X.; Yang, Y. J.; Chen, D. L.; Long, Z. W. Structures, and electronic and spectral properties of single-atom transition metal-doped boron clusters MB$_{24}^-$ (M = Sc, Ti, V, Cr, Mn, Fe, Co, and Ni). *RSC Adv.* **2022**, *12*, 16706−16716.

(46) Yan, L. Large B(7) Triangles in Hollow Spherical Trihedral Metallo-borospheres and Their Endohedral Complexes of B$_{20}$TMn (TM = Sc, Y; n = 3, 4): a Theoretical Characterization. *Inorg. Chem.* **2022**, *61*, 10652−10660.

(47) Đorđević, S.; Radenkovic, S. Electronic structure, stability, and aromaticity of M$_2$B$_6$ (M = Mg, Ca, Sr, and Ba): an interplay between spin pairing and electron delocalization. *Phys. Chem. Chem. Phys.* **2022**, *24*, 5833−5841.

(48) Chen, X.; Chen, T. T.; Li, W. L.; Lu, J. B.; Zhao, L. J.; Jian, T.; Hu, H. S.; Wang, L. S.; Li, J. Lanthanides with Unusually Low Oxidation States in the PrB$_3^-$ and PrB$_4^-$ Boride Clusters. *Inorg. Chem.* **2019**, *58*, 411−418.

(49) Chen, B.; Gutsev, G. L.; Li, D.; Ding, K. Structure and Chemical Bonding in Medium-Size Boron Clusters Doped with Praseodymium. *Inorg. Chem.* **2022**, *61*, 7890−7896.

(50) Dong, X.; Liu, Y. Q.; Tiznado, W.; Cabellos-Quiroz, J. L.; Zhao, J.; Pan, S.; Cui, Z. H. Designing a Four-Ring Tubular Boron Motif through Metal Doping. *Inorg. Chem.* **2022**, *61*, 14553−14559.

(51) Bai, H.; Bai, B.; Zhang, L.; Huang, W.; Zhai, H. J.; Li, S. D. B$_{12}$F$_n^{0/-}$ (n = 1-6) series: when do boron double chain nanoribbons become global minima? *Phys. Chem. Chem. Phys.* **2017**, *19*, 31655−31665.

(52) Tuyet Mai, D. T.; Van Duong, L.; Pham-Ho, M. P.; Nguyen, M. T. Electronic Structure and Properties of Silicon-Doped Boron Clusters BnSi with n = 15−24 and Their Anions. *J. Phys. Chem. C* **2020**, *124*, 6770−6783.

(53) Li, P. F.; Zhai, H. J. Structures and chemical bonding of boron-based B$_{12}$O and B$_{11}$Au clusters. A counterexample in boronyl chemistry. *Phys. Chem. Chem. Phys.* **2022**, *24*, 10952−10961.

(54) Yang, Y. J.; Li, S. X.; Chen, D. L.; Long, Z. W. Structural Evolution and Electronic Properties of Selenium-Doped Boron Clusters SeB$_n^{0/-}$ (n = 3-16). *Molecules* **2023**, *28*, No. 357.

(55) Guo, J. C.; Lu, H. G.; Zhai, H. J.; Li, S. D. Face-capping u3-BO in B$_6$(BO)$_7^-$: boron oxide analogue of B$_6$H$_7^-$ with rhombic 4c-2e bonds. *J. Phys. Chem. A* **2013**, *117*, 11587−11591.

(56) Li, D. Z.; Li, R.; Zhang, L. J.; Ou, T.; Zhai, H. J. Planar B$_3$S$_2$H$_3^-$ and B$_3$S$_2$H$_3$ clusters with a five-membered B$_3$S$_2$ ring: boron-sulfur hydride analogues of cyclopentadiene. *Phys. Chem. Chem. Phys.* **2016**, *18*, 21412−21420.

(57) Li, D. Z.; Bai, H.; Ou, T.; Chen, Q.; Zhai, H. J.; Li, S. D. Planar dicyclic B$_6$S$_6$, B$_6$S$_6^-$, and B$_6$S$_6^{2-}$ clusters: boron sulfide analogues of naphthalene. *J. Chem. Phys.* **2015**, *142*, No. 014302.

(58) Zhao, L.-J.; Xu, X.-L.; Xu, H.-G.; Feng, G.; Zheng, W.-J. Structural and bonding properties of BS$^{-/0}$ and BS$_3^{-/0}$. *New J. Chem.* **2018**, *42*, 16021−16026.

(59) Adamo, C.; Barone, V. Toward reliable density functional methods without adjustable parameters: The PBE0 model. *J. Chem. Phys.* **1999**, *110*, 6158−6170.

(60) Lv, J.; Wang, Y.; Zhu, L.; Ma, Y. Particle-swarm structure prediction on clusters. *J. Chem. Phys.* **2012**, *137*, No. 084104.

(61) Krishnan, R.; Binkley, J. S.; Seeger, R.; Pople, J. A. Self-consistent molecular orbital methods. XX. A basis set for correlated wave functions. *J. Chem. Phys.* **1980**, *72*, 650−654.

(62) Li, P.; Du, X.; Wang, J. J.; Lu, C.; Chen, H. Probing the Structural Evolution and Stabilities of Medium-Sized MoBn0/− Clusters. *J. Phys. Chem. C* **2018**, *122*, 20000−20005.

(63) Jin, S.; Chen, B.; Kuang, X.; Lu, C.; Sun, W.; Xia, X.; Gutsev, G. L. Structural and Electronic Properties of Medium-Sized Aluminum-Doped Boron Clusters AlBn and Their Anions. *J. Phys. Chem. C* **2019**, *123*, 6276−6283.

(64) Ren, M.; Jin, S.; Wei, D.; Jin, Y.; Tian, Y.; Lu, C.; Gutsev, G. L. NbB$_{12}^-$: a new member of half-sandwich type doped boron clusters with high stability. *Phys. Chem. Chem. Phys.* **2019**, *21*, 21746−21752.

(65) Tian, Y.; Wei, D.; Jin, Y.; Barroso, J.; Lu, C.; Merino, G. Exhaustive exploration of MgBn (n = 10-20) clusters and their anions. *Phys. Chem. Chem. Phys.* **2019**, *21*, 6935−6941.

(66) Frisch, M. J.; Trucks, G. W.; Schlegel, H. B.; Scuseria, G. E.; Robb, M. A.; Cheeseman, J. R.; Scalmani, G.; Barone, V.; Petersson, G. A.; Nakatsuji, H.et al. *Gaussian 16*; Gaussian Inc.: Wallingford, CT, 2016.

(67) Lu, T.; Chen, F. Multiwfn: A multifunctional wavefunction analyzer. *J. Comput. Chem.* **2012**, *33*, 580−592.

(68) Humphrey, W.; Dalke, A.; Schulten, K. VMD: Visual molecular dynamics. *J. Mol. Graphics* **1996**, *14*, 33−38.

(69) Alexandrova, A. N.; Boldyrev, A. I.; Zhai, H.-J.; Wang, L.-S. All-boron aromatic clusters as potential new inorganic ligands and building blocks in chemistry. *Coord. Chem. Rev.* **2006**, *250*, 2811−2866.

(70) Becke, A. D.; Edgecombe, K. E. A simple measure of electron localization in atomic and molecular systems. *J. Chem. Phys.* **1990**, *92*, 5397−5403.

(71) Chen, Q.; Li, W. L.; Zhao, Y. F.; Zhang, S. Y.; Hu, H. S.; Bai, H.; Li, H. R.; Tian, W. J.; Lu, H. G.; Zhai, H. J.; Li, S. D.; Li, J.; Wang, L. S. Experimental and theoretical evidence of an axially chiral borospherene. *ACS Nano* **2015**, *9*, 754−760.

(72) Bauernschmitt, R.; Ahlrichs, R. Treatment of electronic excitations within the adiabatic approximation of time dependent density functional theory. *Chem. Phys. Lett.* **1996**, *256*, 454−464.